



**HAL**  
open science

## On the determination of the elastic constants of carbon fibres by nanoindentation tests

T. S. Guruprasad, Vincent Keryvin, Ludovic Charleux, Jean-Pierre Guin,  
Olivier Arnould

► **To cite this version:**

T. S. Guruprasad, Vincent Keryvin, Ludovic Charleux, Jean-Pierre Guin, Olivier Arnould. On the determination of the elastic constants of carbon fibres by nanoindentation tests. *Carbon*, 2021, 173, pp.572-586. 10.1016/j.carbon.2020.09.052 . hal-03027583

**HAL Id: hal-03027583**

**<https://hal.science/hal-03027583v1>**

Submitted on 27 Nov 2020

**HAL** is a multi-disciplinary open access archive for the deposit and dissemination of scientific research documents, whether they are published or not. The documents may come from teaching and research institutions in France or abroad, or from public or private research centers.

L'archive ouverte pluridisciplinaire **HAL**, est destinée au dépôt et à la diffusion de documents scientifiques de niveau recherche, publiés ou non, émanant des établissements d'enseignement et de recherche français ou étrangers, des laboratoires publics ou privés.

# On the determination of the elastic constants of carbon fibres by nanoindentation tests

T.S. Guruprasad <sup>a</sup>, V. Keryvin <sup>a,\*</sup>, L. Charleux <sup>b</sup>, J.-P. Guin <sup>c</sup>, O. Arnould <sup>d</sup>

<sup>a</sup> Univ. Bretagne Sud, UMR CNRS 6027, IRDL, F-56321, Lorient, France

<sup>b</sup> Univ. Savoie-Mont Blanc, EA 4114, SYMME, F-74000, Annecy, France

<sup>c</sup> Univ. Rennes 1, UMR CNRS 6251, IPR, F-35042, Rennes, France

<sup>d</sup> Univ. Montpellier 2, UMR CNRS 5508, LMGC, F-34095, Montpellier, France

## A B S T R A C T

Nano-indentation instrumented tests are carried out at shallow depths on PAN-based and MPP-based carbon fibres. Indentation moduli are obtained by performing the tests at ten different measured orientations with respect to the fibre axis. They are used to identify the elastic constants of the fibres, assuming a transversely isotropic behaviour, by minimising a cost function between measured and estimated values. Inconstancies between the identified in-plane shear and transverse moduli and reported literature values are pointed out, and some drawbacks of the nano-indentation method are highlighted. An improved method taking into account the buckling mechanisms of crystallites at stake during the indentation process, and visible in the hysteretic behaviour of force-penetration nano-indentation curves, is proposed. It allows to identify values of elastic constants that are in accordance with literature values. These elastic properties of carbon fibres are in turn used to estimate the elastic properties of epoxy matrix composites containing these fibres. Very good agreement is found with experimentally available values of unidirectional ply properties. An excellent correlation between experiments and Finite Element Analyses of the indentation response of carbon fibres is eventually found.

### Keywords:

Carbon fibres

Anisotropy

Nanoindentation

Buckling

Identification

Elasticity

## 1. Introduction

With increasing use of composites in many structural applications, carbon fibre composites are extensively used due to their unique properties of high tensile strength, high modulus, and lower strength to weight ratio. Carbon fibres are predominantly employed as reinforcements in composites, widely known as carbon fibre reinforced polymer (CFRP) composites. Due to these advantages, CFRP are employed in many structural applications such as in the aerospace, automotive, naval industries and also in sports applications.

Carbon fibres are highly anisotropic due to their nanostructure inherited from their processing, containing both crystalline and amorphous phases [1] with varying dimensional features. They have a very high tensile modulus in the axial direction and a much lower tensile modulus in the direction perpendicular to their axis. To design composites, the knowledge of elastic properties of carbon

fibres is essential to predict the mechanical response of CFRP. Indeed, multi-scale modelling is more and more employed either for homogenisation (overall properties) or localisation (damage and fracture). Moreover, finding new types of carbon fibres also require to master their structure-properties relationships. Usually, carbon fibres are assumed to be transversely isotropic materials for their elastic behaviour, so that one needs to determine five independent elastic constants: longitudinal modulus, transverse modulus, in-plane shear modulus, in-plane Poisson's ratio and transverse Poisson's ratio.

The longitudinal modulus can be determined by uniaxial tension tests on single fibres or bundles of fibres, but determining the other two moduli is difficult because of the complications in testing due to the small feature size of the carbon fibre. Also, determining Poisson's ratios is very complicated. Several methods have been used to determine the elastic constants such as tension [2], compression [3], torsion [4,5], ultrasonic measurements [6], nanoindentation [7–10] and AFM indentation tests [11]. Some authors also used other methods such as laser diffraction [12], X-ray diffraction [13], micro-Raman spectroscopy [8] on carbon fibres.

In this study, we focus on nano-indentation because of its

\* Corresponding author.

E-mail address: [vincent.keryvin@univ-ubs.fr](mailto:vincent.keryvin@univ-ubs.fr) (V. Keryvin).

obvious advantages. This experimental method requires less difficult sample preparation and allows a large number of tests to be performed to obtain repeatable and accurate results. It allows the simple measurement of an indentation modulus which can be used to determine specific elastic parameters [14], especially on small samples. However, in the case of an anisotropic behaviour such as that of carbon fibres, difficulties in analysing the nanoindentation results arise. The indentation modulus depends on the whole set of elastic constants. Determining this complete set of elastic constants requires many more experiments as well as theoretical and numerical forward and reverse analyses. Delafargue and Ulm [15] gave useful approximations for computing the indentation modulus, but only for two indentation directions with respect to the fibre axis, i.e. longitudinal and transverse directions. Vlassak et al. [16] proposed a comprehensive determination of the indentation modulus for an anisotropic material whatever the indentation direction.

Recently, Csanádi et al. [10] performed nanoindentation experiments at two orientations ( $0^\circ$  and  $90^\circ$ ) on a standard modulus PAN-based carbon fibre. They pointed out that the  $0^\circ$  supposed orientation was closer to  $14^\circ$ , requiring to measure this angle adequately. They determined the transverse and the in-plane shear moduli using Vlassak et al. [16] solutions. They noted a good agreement for both moduli with literature values [6,8]. Yet, for the in-plane shear modulus there exists a 70% difference (see [10, Table 1]). More recently, Duan et al. [11] performed AFM-indentation experiments at two orientations ( $0^\circ$  and  $90^\circ$ ) on three different PAN-based carbon fibres. They also determined the transverse and the in-plane shear moduli using Swanson [17] solution. They noted discrepancies with published data for the transverse modulus and compared their shear modulus values to that of Csanádi et al. [10] mentioned hereinbefore. *To our opinion, a clear and systematic comparison of the values of these two moduli, identified via nano-indentation techniques, with available reported data is missing in literature.*

Since carbon fibres show strong anisotropy between longitudinal and transverse directions, testing only at two directions might be not sufficient to accurately determine the elastic constants. To get the complete set of elastic constants, the fibres are to be tested at varying orientations. Also, because the fibres are small, the correct orientation angle of the fibre has to be measured since some small error in the fibre orientation might propagate into big error in the determined elastic constants. Jäger et al. [18] performed nanoindentation tests on wood cell walls to determine their elastic properties at varying angles between the indentation direction and the direction of cellulose microfibrils. They used the estimations of Vlassak et al. [16] to determine the values of the three elastic moduli by minimising a cost function between estimated and measured values. *To our opinion, an enhanced and comprehensive set of indentation moduli at varying angles, measured adequately, is missing in literature for identifying the elastic constants of carbon fibres, not only for PAN-based fibres but also for MPP-based ones.*

From the reported literature works, the motivations of this original work are twofold. Firstly, a comprehensive campaign of nanoindentation tests is made on 10 different (measured) orientation angles for four different carbon fibres. Three fibres are PAN-based with standard, intermediate or high modulus, and the last one is MPP-based of ultra high modulus. A careful analysis of the raw results is made for extracting a complete set of indentation moduli with respect to the orientation angles. The forward estimations of the indentation modulus of Vlassak et al. [16] from the elastic constants of the fibres are used and incorporated in a reverse analysis minimising the error between measured and estimated indentation moduli. Secondly, the identified elastic parameters are systematically compared to values reported in literature. They are

also used for estimating elastic ply properties of CFRP, in turn compared to existing reported values, which is another originality of this paper. The clear existence of some inconsistencies will pave the way for interpreting the deformation mechanisms at stake during nano-indentation in the light of the ultrastructure of carbon fibres. The disadvantages of identifying elastic constants of carbon fibres by nanoindentation are discussed. An improved protocol is proposed to soundly identify two relevant parameters usually difficult to measure, the in-plane shear modulus and the transverse modulus. A Finite Element Analysis of the indentation response of carbon fibres is eventually made.

## 2. Materials and methods

### 2.1. Materials

In this study, four different types of carbon fibres are chosen: three fibres are of PAN precursor type (polyacrylonitrile), and the last one is MPP (meso-phase pitch) precursor type. All the fibres are part of cured composite prepregs with an epoxy matrix having a fibre volume fraction ( $V_f$ ) of around 55 %. The PAN-based fibres are UTS50 (Teijin, standard modulus), IM2C (Hexcel, intermediate modulus), HR40 (Mitsubishi, high modulus), and the MPP-based fibre is K637 (Mitsubishi, ultra high modulus). The diameters of the fibres are  $7\ \mu\text{m}$  (UTS50),  $5.2\ \mu\text{m}$  (IM2C),  $6\ \mu\text{m}$  (HR40), and  $11\ \mu\text{m}$  (K637) respectively. Their longitudinal moduli are 240 GPa (UTS50), 296 GPa (IM2C), 375 GPa (HR40) and 640 GPa (K637) [19–22].

### 2.2. Experimental methods

#### 2.2.1. Surface preparation and microscopic analysis

To study the anisotropy in the carbon fibres, initially, the fibres are cut at varying orientation angles ( $\theta$ ) between  $0^\circ$  (fibre axis) and  $90^\circ$  (transverse direction) in steps of  $10^\circ$  with respect to the fibre axis using a diamond disc cutter. The required surface quality for the nanoindentation tests is achieved by polishing the samples with silicon carbide papers of 1000, 2000, and 4000 grit and then with diamond suspensions having particle sizes of  $3\ \mu\text{m}$  and  $1\ \mu\text{m}$  and finally, with colloidal silica of particle size of  $0.03\ \mu\text{m}$ .

Due to machining and polishing procedures followed during the surface preparation, the achievement of a precise orientation angle is difficult, and the actual orientation may differ from the cutting angle ( $\theta_C$ ). To determine the exact orientation angle, a microscopy analysis is performed on the polished surface using a scanning electron microscopy (SEM, JEOL JSM 6301 F). The SEM images are captured for all the orientations, and then they are digitised using ImageJ software [23] to measure the dimensions of the cross sections of the fibres. The actual angle ( $\theta_M$ ) is calculated from the dimensions of these cross sections. For a fibre with orientation angle,  $\theta_C = 0^\circ$ , the shape of the fibre is a circle and for  $\theta_C = 90^\circ$ , it is a rectangle as it is perpendicular to the axis and for rest of the angles, it is an ellipse. Fig. 1 shows SEM images of the carbon fibres with orientation angles  $\theta_C = 0^\circ$  and  $70^\circ$  respectively. For a fibre with orientation angle between  $\theta_C = 0^\circ - 80^\circ$ , the major and minor axes of the ellipse are measured from their respective SEM images. The angle is calculated using the relation  $\theta_M = \cos^{-1}\left(\frac{b}{a}\right)$ , where  $a$  and  $b$  are the major and minor axes of the ellipse. Fig. 1(c) shows the schematic of the ellipse and the method for calculating the actual orientation angle from the carbon fibre cross section.

About 200 or more fibres were analysed to obtain the measured orientation angle. As for a possible effect of the fibre undulation on the measured orientation angle, we do not consider it, since in

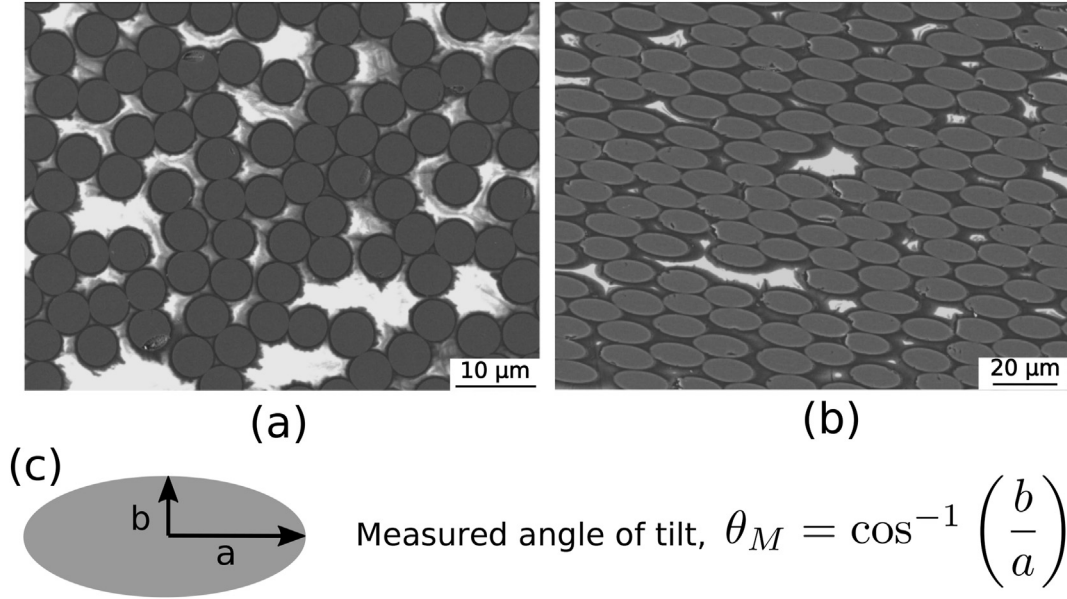


**Fig. 1.** SEM images of carbon fibre type IM2C with cutting angle ( $\theta_c$ ) (a)  $0^\circ$  and (b)  $70^\circ$ . (c) Schematic of an ellipse with its dimensions used to calculate the actual angle of tilt ( $\theta_M$ ). (A colour version of this figure can be viewed online.)

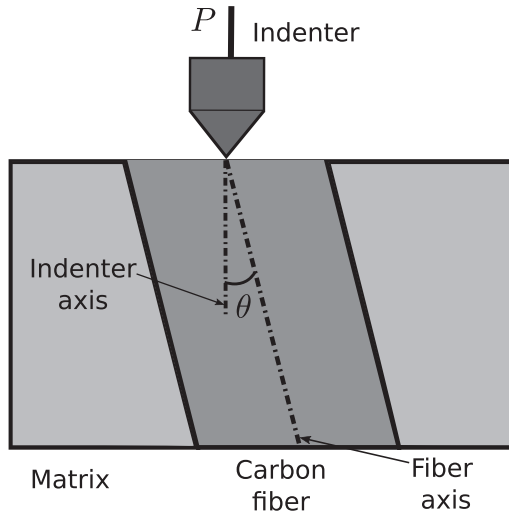


**Fig. 2.** A schematic of an indentation test carried out on a carbon fibre orientated with an angle ( $\theta$ ) with respect to its axis. (A colour version of this figure can be viewed online.)

previous works we measured waviness angles of around  $1^\circ$  in unidirectional plies of composites for the materials studied in the present paper [24].

### 2.2.2. Nanoindentation tests

Nanoindentation tests are conducted on the four different carbon fibres with varying orientation angle between  $\theta_c = 0^\circ$  and  $90^\circ$ . Fig. 2 shows the schematic of the indentation test performed on a carbon fibre cross section, where the fibre is orientated with an angle  $\theta$  with respect to the indentation axis. The tests are performed using Hysitron TI 950 Triboindenter (for IM2C and HR40) and MTS Nano XP Nanoindenter (for UTS50 and K637), with a diamond (modified) Berkovich tip, in load controlled mode with the following sequence: 10 s to reach the maximum force, 10 s of

holding time and 10 s to unload at zero force. The force and penetration into the sample are recorded. For HR40 fibre both apparatus were used, which gave the same results (force-penetration curves and extracted indentation moduli). The advantages of the TI950 are that i) it is possible to get the raw signals from the sensors especially the displacement one without corrections such as tip area calibration which is useful when comparing with finite-element simulations, and ii) the surface can be imaged by the tip before and after the test. In situ scanning probe microscopy mode (SPM) is used, where the desired position is selected, and topographic images before and after the tests are captured [25].

All the tests are performed up to shallow indentation depths lower than  $\sim 150\text{nm}$ ; at higher depths, the surrounding material may influence the results as reported by Csanádi et al. [10]. The contact stiffness,  $S$ , is measured by fitting the unloading part of the indentation curve (force-penetration) and taking its derivative at the maximum penetration depth. This makes it possible to determine the effective indentation modulus  $M_{eff}$ , as given by Oliver and Pharr [14]:

$$S = \frac{2}{\sqrt{\pi}} \sqrt{A_c} M_{eff} \quad (1)$$

where  $A_c$  is the projected contact area, which is a function of the contact depth, calibrated by measurements on a fused silica standard. To take into account the deformability of the diamond indenter, we have:

$$\frac{1}{M_{eff}} = \frac{1 - \nu_i^2}{E_i} + \frac{1}{M} \quad (2)$$

where  $M$  is the indentation modulus of the material,  $E$  (1100 GPa) and  $\nu_i$  (0.07) are the Young's modulus and Poisson's ratio of the indenter respectively.

For each orientation angle, at least 10 indentation tests are performed on the centre of 10 different fibres and is repeated for four different types of fibres. The indentation hardness ( $H$ ) is also taken as the ratio between the maximum applied force and the projected contact area. An average indentation modulus is

associated to the average value of the orientation angle.

### 2.3. Analytical and computational methods

#### 2.3.1. Theoretical models for anisotropic indentation

With the aim of determining the elastic properties of the material by nanoindentation, the indentation modulus can be related to the elastic constants for an isotropic material as

$$M = \frac{E}{1 - \nu^2} \quad (3)$$

where  $E$  and  $\nu$  are the elastic modulus and Poisson's ratio of the material respectively.  $M$  is independent of the indentation direction for isotropic materials.

In the case of anisotropic materials, the relation between indentation modulus and the elastic constants is more complicated, because it also depends on the indentation direction. Approximate closed-form expressions between the indentation modulus and the elastic constants ( $C_{ij}$ ) for transversely isotropic materials are proposed by Delafargue and Ulm [15], and the solution can be used when the indentation direction is the direction of one of the principal material axes. The solution of the indentation modulus is available only at two independent directions, i.e. at the longitudinal cross section,  $0^\circ$  and transverse cross section,  $90^\circ$ . The indentation modulus in the longitudinal cross section is given by:

$$M_{0^\circ} = 2\sqrt{\frac{C_{31}^2 - C_{13}^2}{C_{11}} \left( \frac{1}{C_{44}} + \frac{2}{C_{31} + C_{13}} \right)^{-1}} \quad (4)$$

where 3 is the fibre axis ( $0^\circ$ ) and.  $C_{31} = \sqrt{C_{11}C_{33}}$ .

Similarly, the indentation modulus in the transverse cross section is given as:

$$M_{90^\circ} = \sqrt{M_{12}M_{13}} \quad (5)$$

where,  $M_{12} = \sqrt{\frac{C_{11}}{C_{33}}}M_3$  and.  $M_{13} = \frac{C_{11} - C_{12}^2}{C_{11}}$ .

Another well-defined solution scheme for general anisotropic elastic materials was proposed by Vlassak et al. [16]. The major advantage of this solution over that of Delafargue and Ulm [15] solution is that it provides solution for any angle between  $0^\circ$  and  $90^\circ$ . So, the complete solution relates the indentation modulus with the elastic properties of the material as well as the indentation direction. The indentation modulus is given by:

$$M = \frac{1}{\alpha(e, \Phi) (1 - e^2)^{\frac{3}{4}}} \quad (6)$$

With the assumption of an elliptical contact area formed with the conical indenter, the function  $\alpha(e, \Phi)$  relates to eccentricity ( $e$ ) of the contact ellipse and angle ( $\Phi$ ) between the major axis of the ellipse and the reference direction of a function  $h$ , which is the angle dependent part of the surface Green's function linked to normal contact point loading of an elastic half-space. A minimisation of  $\alpha(e, \Phi) \times E(e)$  is made to find  $e$  and  $\Phi$ , where  $E$  is the complete elliptic integral of the second kind.

An approximation of the complete solution can be made. It consists in assuming a circular contact.  $h$  is developed into a Fourier series expansion with  $h_0$  being the constant term. This approximation gives:

$$M = \frac{1}{\pi h_0} \quad (7)$$

All estimations are implemented in a Python script and compared for an anisotropic material (see Appendix A for details). It is found that results obtained from the approximate solution assuming circular contact is much faster. Comparing the different estimations, it can be seen that the indentation modulus is the same for all solutions. Therefore, the solution assuming circular contact is used in this paper, especially since optimisations will be made (see below).

#### 2.3.2. Determination of elastic constants via reverse analysis

Using the numerical relations between indentation modulus and the elastic constants, a minimisation procedure is used for Vlassak et al. [16] circular contact approximate solution to determine the elastic constants, where the indentation moduli from experiments are compared with numerically predicted values. The procedure adopted is similar to that of Jäger et al. [18], where they determined the elastic constants of wood cell walls. We assume the elastic behaviour of carbon fibres to be transversely isotropic. The elastic constants are the longitudinal and transverse moduli ( $E_l$  and  $E_t$ ), the in-plane shear modulus ( $G_{lt}$ ) and the in-plane and transverse Poisson's ratios ( $\nu_{lt}$  and  $\nu_t$ ). The value of  $E_l$  is known, as it is provided by the carbon fibre manufacturers [19–22]. Both Csanádi et al. [10] and Duan et al. [11] showed from their parametric studies that the influence of Poisson's ratios of carbon fibres on indentation modulus is negligible. Jäger et al. [26] found the same on wood fibres. Here the Poisson's ratios values are assumed to be 0.274. Therefore, only the elastic moduli  $E_t$ , and  $G_{lt}$ , are to be determined.

The objective function  $R$  to be minimised is,

$$R^2 = \frac{\sum_{i=1}^n [M_{exp}(\theta_i) - M_{num}(E_t, G_{lt}, \theta_i)]^2}{\sum_{i=1}^n [M_{exp}(\theta_i)]^2} \quad (8)$$

where  $n$  is the number of orientation angles,  $M_{exp}$  is the indentation modulus from experiments,  $\theta_i$  is the orientation angle,  $M_{num}$  is the numerically predicted value of indentation modulus. A Nelder-Mead method (Simplex method) is used for the minimisation procedure.

#### 2.3.3. Finite element modelling

Finite element simulations of the indentation test between a diamond tip and a carbon fibre were carried out using the commercial implicit solver Abaqus/Standard [27]. Fig. 3 shows the numerical model.

The indenter is a three dimensional (3D) deformable sphero-conical body with a truncated length  $\Delta h = 20$  nm (the reasons for using such a value are explained later in § 3.1.1) and cut by a sphere of radius  $R_i = 10\mu\text{m}$  at its far end. The included half-angle of the cone is taken as  $70.29^\circ$  to match the theoretical projected area function of the modified Berkovich indenter. The sample is 3D and consists in a half sphere of radius  $R_s = 70\mu\text{m}$ . It contains the carbon fibre at  $\theta = 90^\circ$  of radius  $R_f$  and a surrounding material taken as the unidirectional composite (see § 2.1). The outer dimensions of both bodies  $R_i$  and  $R_s$  are high enough to minimise the effect of the boundary conditions. Given the symmetries of the model, only a quarter is simulated. The indenter and the sample are meshed respectively with 10,268 and 22,956 tetrahedrons. Both meshes are produced by GMSH (version 4.5.5) [28]. Meshes and models are created using the Python frameworks Hardness [29] and Argiope [30]. The contact between the indenter and the fibre is taken as frictionless. The simulations are displacement controlled. The diamond indenter follows an isotropic elastic behaviour (Young's modulus of 1100 GPa and Poisson's ratio of 0.07). Both the



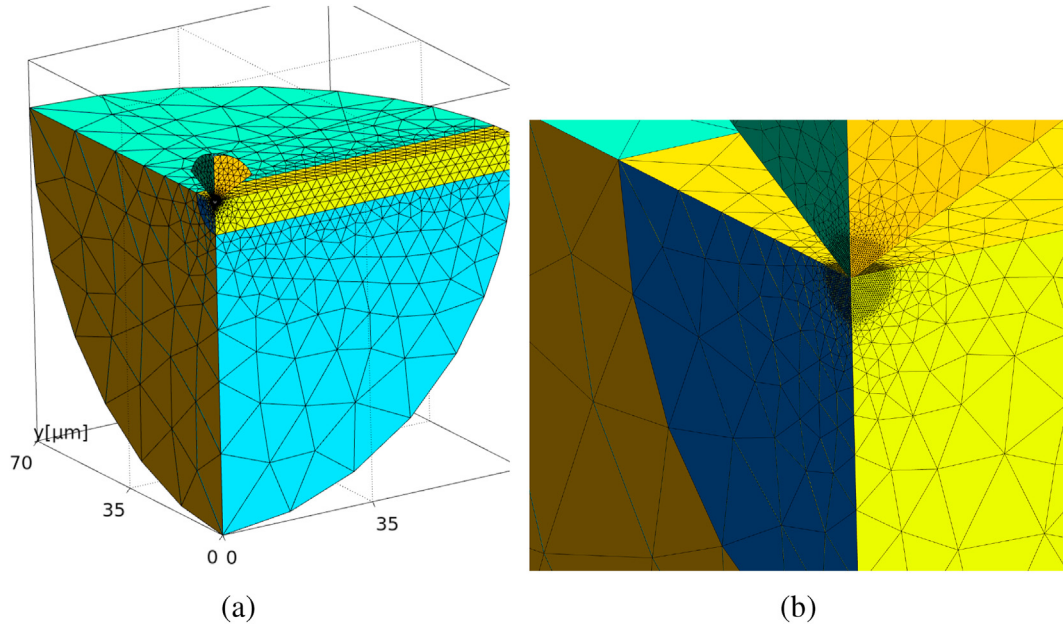


**Fig. 3.** Representation of the 3D FEM model with its mesh introducing the deformable sphero-conical elastic indenter, the carbon fibre cut at  $90^\circ$  and the surrounding medium around the fibre. (a) The model is represented as a whole in order to highlight its dimensions. (b) The contact area between the indenter and the fibre is enlarged. The fine mesh areas of the indenter and the fibre are visible. (A colour version of this figure can be viewed online.)

surrounding material and the carbon fibre have a transversely isotropic elastic behaviour.

### 3. Results

#### 3.1. Nanoindentation results

##### 3.1.1 Force-displacement curves and imprints.

Fig. 4 shows representative plots of force ( $P$ ) versus the indentation depth ( $h$ ) for all carbon fibres with varying orientation angles  $\theta_C$  between  $0^\circ$  and  $90^\circ$  from nanoindentation tests. The  $P-h$  curves are plotted with the measured orientation angle  $\theta_M$ , which is the actual angle measured from the SEM images. For example, for IM2C, from the microscopic analysis, we found that for a fibre cut with an orientation angle  $\theta_C = 0^\circ$ , the measured angle was found to be  $\theta_M = 12^\circ$ . The difference is due to experimental constraints in the preparation of the sample. The  $P-h$  curves show strong anisotropic behaviour between the longitudinal and transverse directions, and the behaviour is in agreement with other carbon fibres tested by various authors [10,11,31]. To produce the same indentation depth for the IM2C fibres oriented between  $0^\circ$  and  $90^\circ$ , the force supported by the fibre with angle  $12^\circ$  is highest, which is nearly three times in comparison to the  $90^\circ$  one.

The  $P-h$  curves for the PAN-based fibres exhibit a reversible or quasi reversible behaviour along with a hysteretic behaviour. Those for MPP fibre show, at the contrary, some plastic deformation. Fig. 5(a) presents a selective view of Fig. 4 for IM2C and the two extreme angles. The mechanical behaviour is highly reproducible from one fibre to another. The hysteretic behaviour is very much pronounced for  $\theta_C = 0^\circ$ . Some plastic deformation (less than 5 nm in residual depth) can be seen from the indentation impression observed on SPM images in Fig. 5(b). In sharp contrast, in the case of fibres oriented with an orientation angle  $\theta_M = 90^\circ$ ,  $P-h$  curves show negligible hysteresis, and they are nearly elastic. From the SPM image on Fig. 5(c), it is clear that there is no indentation print after unloading and that the surface of the sample returns to its original shape.

To get a clearer view on the different curves of Fig. 4, a way to sort them out is to extract an indentation parameter called the loading pre-factor,  $C$ , which describes the parabolic nature of the loading curve  $P = C \cdot h^2$ . This relationship comes from the geometrical self similarity of the sharp indentation test [32]. The value of  $C$  depends on the indented material and the tip geometry. For an isotropic material its value does not depend on the orientation and is therefore constant for a given tip. For an anisotropic material, such as here, for a given tip sharpness, it depends on the orientation angle. However, the indenter tip is not perfect and this relationship holds for high enough penetration depths with respect to the length scale introduced by the imperfect tip. Fig. 6 (a) presents the square root of the force versus the penetration depth where the experimental data were fitted by a linear function for penetration depths higher than 80 nm, which slope gives the square root of the loading pre-factor  $C$ . The extrapolation of this fit to zero force makes it possible to extract a truncated length as explained in Keryvin et al. [33], which is for this tip  $\Delta h = 20$  nm. Geometrically, this truncated length is the distance between the ideal conical tip and the actual indenter tip Fig. 6 (b) shows the variations of  $C$  for all fibres with respect to the orientation angle. For all fibres,  $C$  decreases with increase in the orientation angle up to  $60-70^\circ$ , where it becomes nearly constant.

##### 3.1.2. Indentation parameters

Fig. 7(a) shows the orientation dependence of the indentation modulus, where a strong anisotropic behaviour is noticeable whatever the carbon fibre. The indentation modulus decreases with an increasing orientation angle. However, the contrast between the highest to the lowest indentation modulus is much lower ( $\sim 3$ ) than that of the contrast between longitudinal modulus to transverse modulus of the carbon fibre (more than 10). Indeed, the former is 2.6, 3.2, 3.2 and 3.5, while the latter is 12, 15, 19 and 32, respectively for UTS50, IM2C, HR40 and K637 (assuming  $E_t \sim 20$  GPa for all fibres). From the plot, we can also observe that the lower the longitudinal modulus  $E_l$ , the higher the indentation modulus, whatever the orientation angle. We can see a decreasing trend with

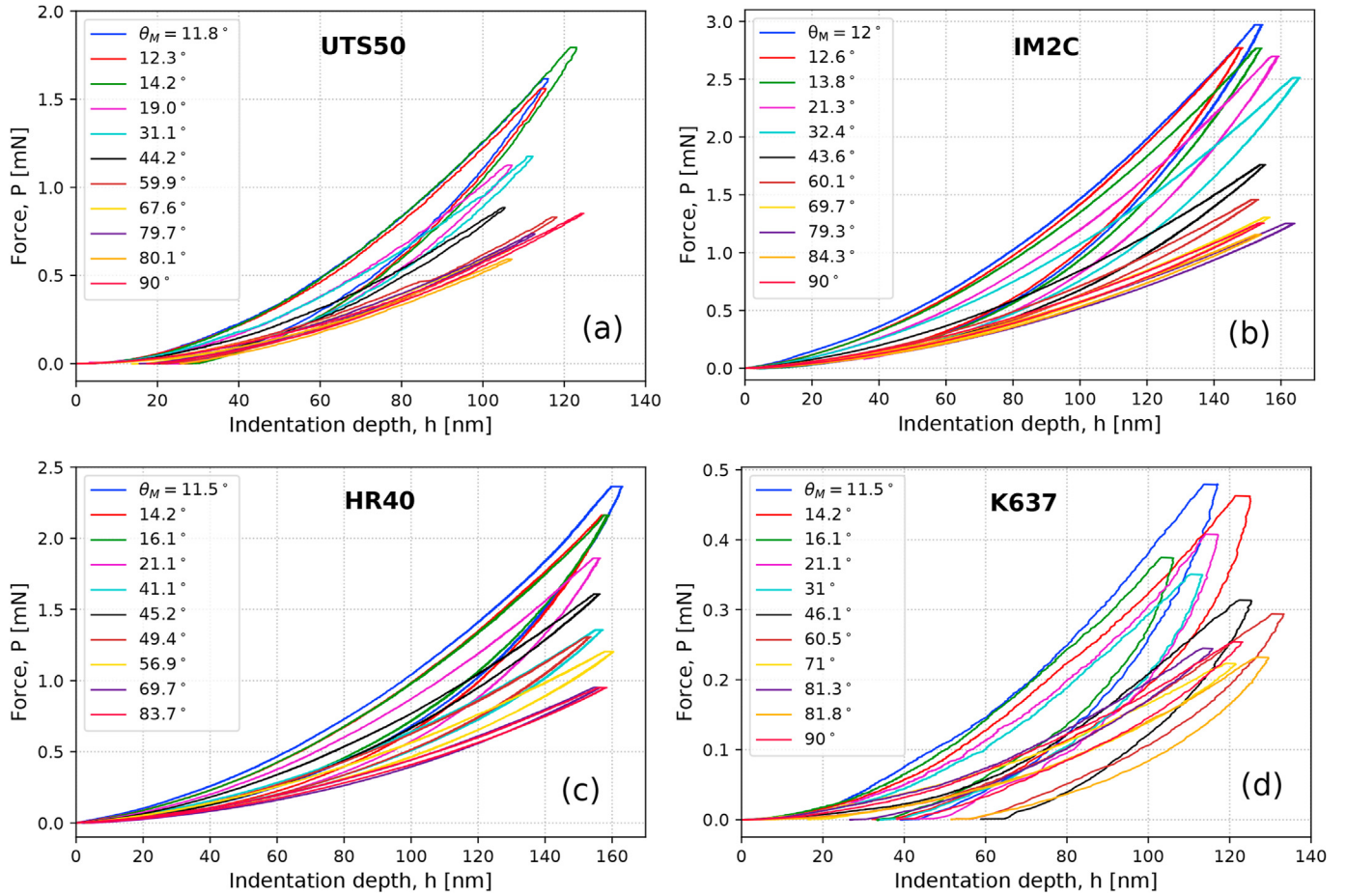


**Fig. 4.** Representative force ( $P$ ) versus indentation depth ( $h$ ) curves from nano-indentation tests on all carbon fibres at various orientation angles for  $\theta_c \in [0; 90^\circ]$ . (A colour version of this figure can be viewed online.)

the increase in the longitudinal modulus between the fibres for all the orientation angles.

A quite similar decreasing trend was observed in the indentation hardness with the orientation angle for all the four fibres, as seen in Fig. 7(b). The anisotropic behaviour is moderate with a contrast between the highest to the lowest hardness value of 1.7 for the three PAN-based fibres and 1.4 for the MPP one. From the plot, we can also observe that the lower the longitudinal modulus  $E_l$ , the higher the indentation hardness, whatever the orientation angle.

For both indentation parameters, the decrease is much faster for the low orientation angles below  $\sim 50^\circ$  and, beyond, the parameters are quasi constant or decrease slightly.

### 3.2. Estimation of elastic parameters

The determined values of elastic constants ( $E_t$  and  $G_{lt}$ ) from minimisation are shown in Table 1 (left side of the table, 'E<sub>l</sub> fixed'). The error  $R$  (Eq. (8)) between estimations ( $M_{num}$ ) and experiments ( $M_{exp}$ ) is  $\sim 6\%$  and  $10\%$  for the PAN-based fibres and MPP-based fibres, respectively. Then, the determined elastic constants make it possible to plot the indentation modulus as a function of the orientation angle, along with the experiments, using the numerical solutions of Vlassak et al [16]. and Delafargue and Ulm [15]. Fig. 8 shows this comparison between experiments and estimations (dark cyan line, 'E<sub>l</sub> fixed'). The fit obtained closely matches with the nanoindentation experiments in accordance with the low minimisation error values. Some discrepancy is however visible for the

MPP fibre Fig. 8 (d). The influence of the cutting angle versus the measured orientation angle on the elastic constants is studied and the results are shown in Appendix B.

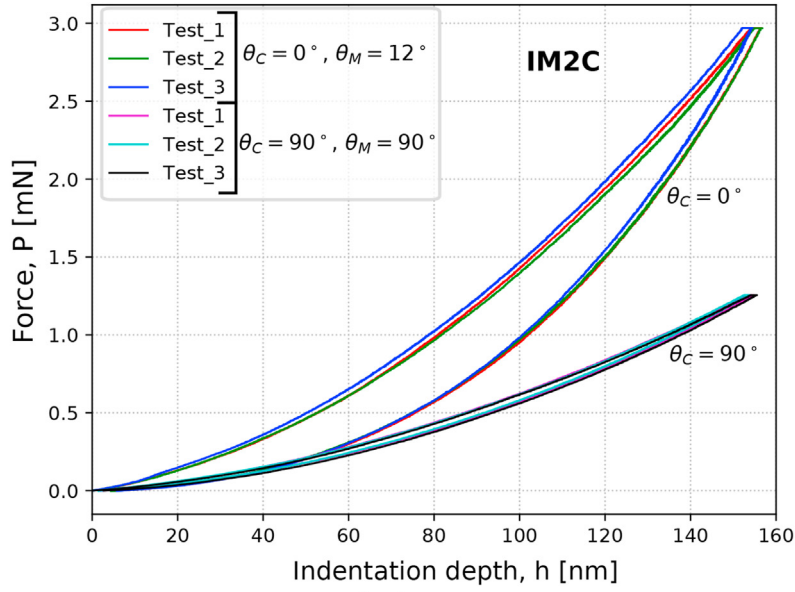
### 3.3. Finite element analyses

The elastic parameters of IM2C fibre in tab:elastic are introduced in the FE model described in § 2.3.3 as well as its radius  $R_f = 2.6 \mu\text{m}$ . The surrounding material (composite with resin and carbon fibres) has the following parameters: longitudinal modulus 168 GPa, transverse modulus 8GPa, in-plane shear modulus 4.5GPa, in-plane Poisson's ratio 0.3, transverse Poisson's ratio 0.3 [34]. The choice of this orientation is motivated by the lowest hysteretic behaviour for all orientation angles. Fig. 9 ('E<sub>l</sub> fixed') shows the comparison between experiment and simulation. The agreement is rather good.

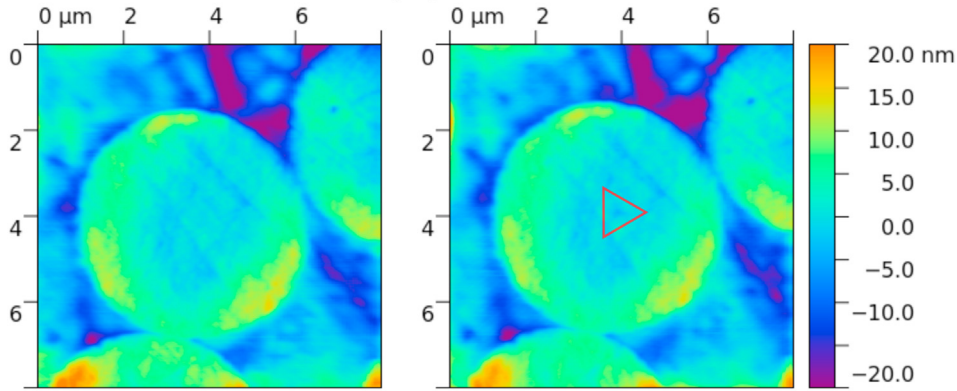
## 4. Discussion

### 4.1. Relevance of nanoindentation results and extracted elastic parameters

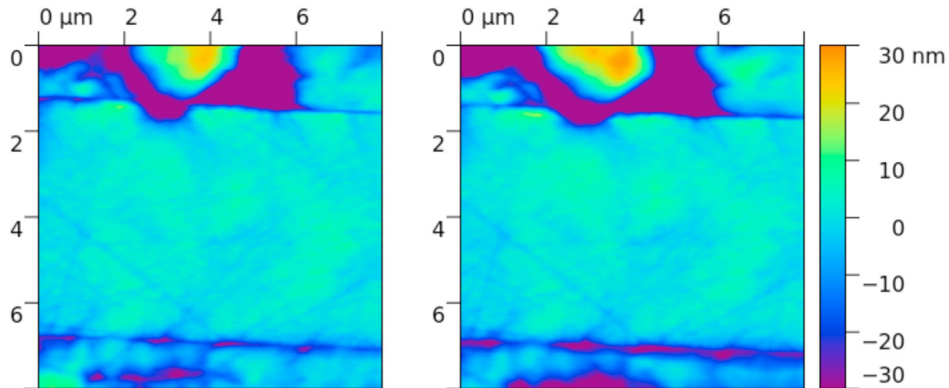
Two elastic constants (transverse modulus  $E_t$  and in-plane shear modulus  $G_{lt}$ ) of four different carbon fibres (3 very different PAN types - standard modulus, intermediate modulus, high modulus fibres - and one of MPP type) were determined from reverse analysis on the indentation moduli obtained by nanoindentation



(a)



(b)



(c)

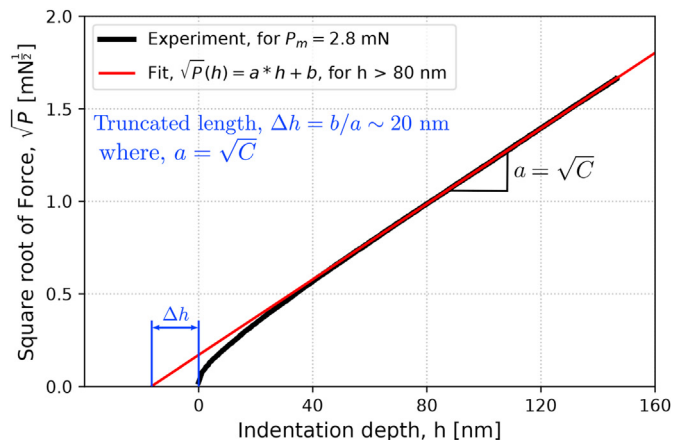
**Fig. 5.** (a) Force versus indentation depth from nanoindentation tests on IM2C carbon fibres at  $\theta_M = 12^\circ$  and  $90^\circ$ . SPM images before and after indentation at (b)  $\theta_M = 12^\circ$  and (c)  $\theta_M = 90^\circ$ . The red triangle highlights the shallow imprint. (A colour version of this figure can be viewed online.)

tests performed at different orientation angles vis-a-vis the fibre axis. In this paragraph, we compare our results with works that used basically the same protocol. Table 2 summarises our results and those from different literature contributions [7,10,11] in terms of indentation moduli of different carbon fibres. Table 3 compiles our results and those from different literature articles [10,11,35] in

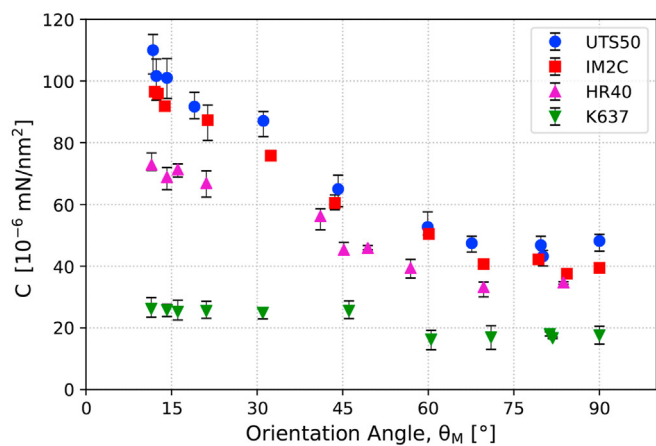
terms of transverse and in-plane shear moduli of different carbon fibres.

Csanádi et al. [10] performed nanoindentation tests on PAN type T300 carbon fibres. They used approximate solutions (see Eqs. (4) and (5)) to determine the two elastic constants from Delafargue and Ulm [15]. The fibres were tested only at two orientations

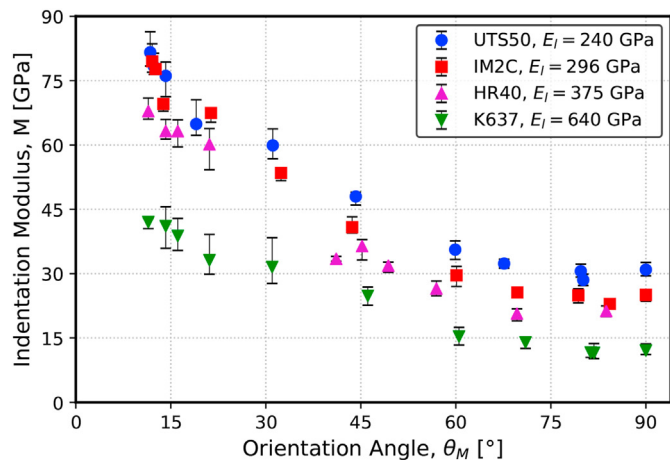




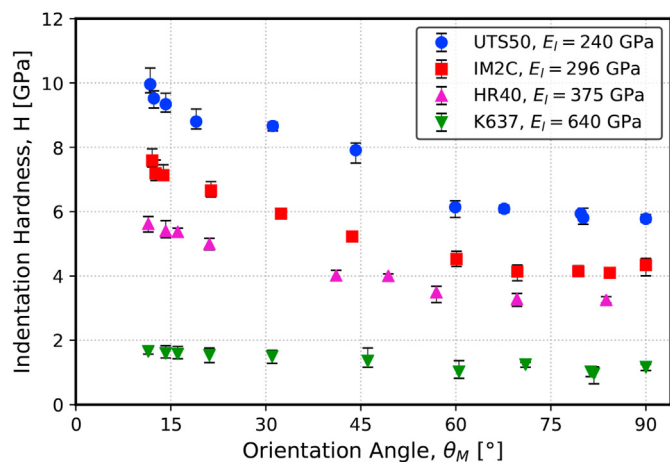
(a)



(b)



(a)



(b)

**Fig. 6.** (a) Example of a plot of the square root of the force versus the indentation depth during the loading stage from indentation test on IM2C fibre. A linear fit for depths higher than 80 nm is extrapolated down to the zero force to give the tip defect in terms of a truncated length  $\Delta h \sim 20$  nm, (b) Plot of  $C$  versus the orientation angle from testing of all four carbon fibres. (A colour version of this figure can be viewed online.)

( $\theta = 0^\circ$  and  $90^\circ$ ) as compared to ours, where we tested more than ten orientations between  $0^\circ$  and  $90^\circ$ . They also corrected the  $0^\circ$  angle into  $14^\circ$  angle by means of AFM measurements like we made for all our orientation angles. Their determined values were  $E_t = 27.6$  GPa and  $G_{lt} = 10.9$  GPa, which are very close to our values with similar carbon fibre type UTS50. They also showed by FEM that performing 150 nm deep indentations made it possible to remove the influence of the surrounding environment of the fibre. Since we have used the same conditions, our results are also free of the influence of the surrounding material influence.

Duan et al. [11] carried out a similar investigation very recently on three different types of PAN carbon fibres (T800, IMS65, M60J), where the fibre surface is prepared by FIB machining, and nano-indentation experiments (NI) were again performed only at two orientation angles ( $0^\circ$  and  $90^\circ$ ). They pointed out that indentation moduli in the  $0^\circ$  orientation were underestimated by nano-indentation tests ( $\sim 45$  GPa) because of buckling issues. They proposed to use AFM to perform spherical nano-indentations at shallower depths giving  $\sim 100$  GPa indentation moduli. Let us note that both our results and those of Csanádi et al. [10] report

**Fig. 7.** Results from the nanoindentation experiments on four different carbon fibres. (a) Indentation modulus ( $M$ ) versus the orientation angle ( $\theta_M$ ), and (b) indentation hardness ( $H$ ) versus the orientation angle ( $\theta_M$ ).

indentation moduli for the  $0^\circ$  orientation (actually  $\sim 15^\circ$ ) around 70–80 GPa (PAN-based fibres) giving extrapolated values at  $0^\circ \sim 80$ –90 GPa by using nanoindentation tests in disagreement with Duan et al. [11] results. Duan et al. attributed the discrepancy between NI and AFM results to possible nano-buckling of graphene sheets and plastic sliding of graphite basal planes. Therefore, there exists the possibility for our results and those of Csanádi et al. [10] to be in between NI results of Duan et al. [11] and their AFM results since our smallest orientation angle is not  $0^\circ$  but  $\sim 15^\circ$ , for which the underlying mechanisms would be of lesser extent. Duan et al. [11] used the numerical solutions given by Swanson [17] to determine the elastic constants. The  $G_{lt}$  values are in good agreement with our results (see Table 3,  $E_t$  fixed) and those of Csanádi et al. [10] when comparing similar types of fibres. Especially, we found the same ranking: the higher the axial modulus of the fibre ( $E_t$ ) the lower the in-plane shear modulus  $G_{lt}$ . As for the  $E_t$  values, the authors [11] wrote that they are in line with those of Maurin et al. [7]. These results are yet very different from our results and those of Csanádi et al. [10]. Let us point out, moreover, that in the work of Maurin et al. [7], the values are transverse indentation moduli and not transverse moduli, where no theory for anisotropic indentation

**Table 1**

Elastic constants determined from minimisation of the cost function  $R$ , see Eq. (8), for the four different types of carbon fibres, and its error  $R$  with respect to the experimental values, when  $E_l$  is fixed (left side) or free (right side). All the elastic constants values are in GPa. The values with +ve and -ve symbols are errors in the estimated values.

Carbon fibre	$E_l$ is fixed, $E_t$ and $G_{lt}$ are free				$E_l, E_t$ and $G_{lt}$ are free			
	$E_l$	$E_t$	$G_{lt}$	Error, R (%)	$E_l$	$E_t$	$G_{lt}$	Error, R (%)
UTS50	240	$32.1^{+0.8}_{-1.1}$	$9.8^{+1.3}_{-0.8}$	5.2	$130^{+6.2}_{-0.9}$	$24.3^{+0.9}_{-0.6}$	$23.4^{+2.0}_{-2.7}$	4.5
IM2C	296	$26.3^{+1.0}_{-1.5}$	$8.1^{+0.4}_{-0.3}$	6.0	$133^{+2.5}_{-0.6}$	$17.7^{+0.9}_{-1.1}$	$25.9^{+0.6}_{-1.1}$	4.0
HR40	375	$26.8^{+0.5}_{-1.5}$	$4.6^{+0.6}_{-0.4}$	6.6	$166^{+13.8}_{-0.2}$	$14.5^{+1.3}_{-0.4}$	$22.9^{+1.4}_{-3.8}$	4.6
K637	640	$21.2^{+3.3}_{-2.4}$	$1.2^{+0.1}_{-0.2}$	10.2	$73.5^{+7.0}_{-5.0}$	$9.6^{+1.9}_{-1.1}$	$13.2^{+0.1}_{-0.9}$	6.2

is used. Therefore our results for  $E_t$  are much more in line with those of Csanádi et al. [10] than with those of Duan et al. [11]. They are also in line with the  $G_{lt}$  ranking. Again, the higher the axial modulus of the fibre ( $E_l$ ) the lower the transverse modulus  $E_t$ .

Ishikawa et al. [5] determined the in-plane shear modulus of both PAN and MPP type fibres with a torsion pendulum device. They found values around 15 GPa for high-strength (T300B) and very high modulus (M60J) PAN-based carbon fibres and 6 GPa for a MPP-based carbon fibre. They also reported, based on literature survey, that  $G_{lt}$  is between 12 and 25 GPa for PAN-based fibres. Kumar et al. [4] found 18.5 GPa with the same technique but the type of carbon fibre is not reported. Csanádi et al. [10] themselves compared the shear modulus they found by nano-indentation ( $\sim 10$  GPa) with acoustic measurements from literature ( $\sim 18$  GPa) and

found a 70% difference (see [10, Table 1]). Our results, as shown in Table 3 ( $E_l$  fixed), as well as those from Csanádi et al. [10] and Duan et al. [11] are clearly close or below 12 GPa, therefore in discrepancy with Ishikawa et al. [5].

Ballard et al. [35] determined the elastic constants of carbon fibres, from reverse analysis on continuous fibres composites elastic moduli, using Mori-Tanaka homogenisation scheme, and also by the finite element approach. From the results shown in Table 3, we observe that the shear modulus values found in Ref. [35], for IM and SM PAN-based fibres, are much higher than those reported from the literature using nanoindentation or AFM, including ours. As for the transverse modulus ( $E_t$ ), their values are basically in line with results from Csanádi et al. [10], Duan et al. [11].

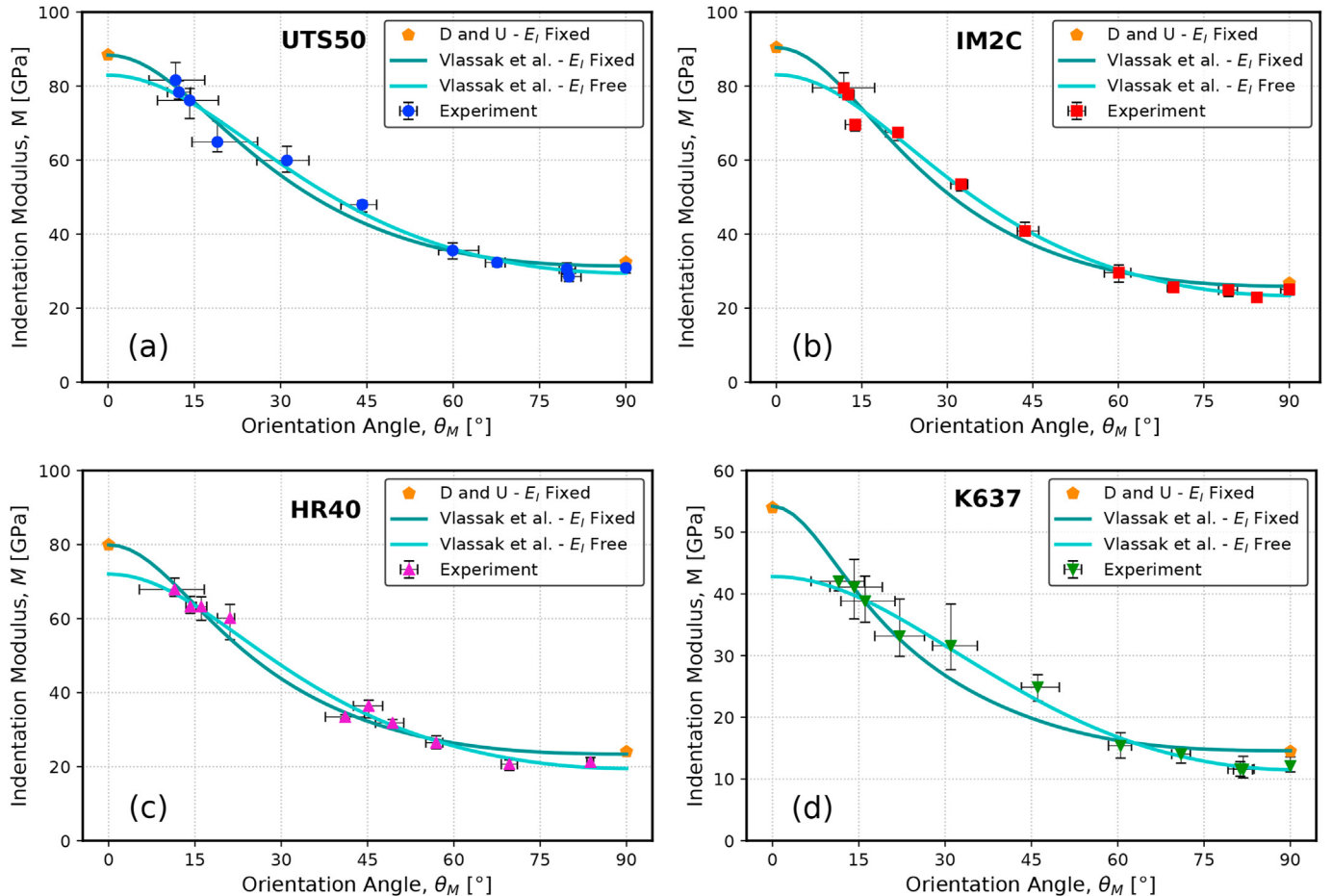


**Fig. 8.** Plots of indentation modulus ( $M$ ) versus orientation angle ( $\theta_M$ ) from nanoindentation experiments, estimations from Delafargue and Ulm [15] (pentagon markers, D and U) and Vlassak et al. [16] (solid lines) for carbon fibres of type (a) UTS50, (b) IM2C, (c) HR40, and (d) K637. The latter dark cyan line is for the minimisation with two parameters ( $E_l$  fixed) while the light cyan line is for three ( $E_l$  free). (A colour version of this figure can be viewed online.)

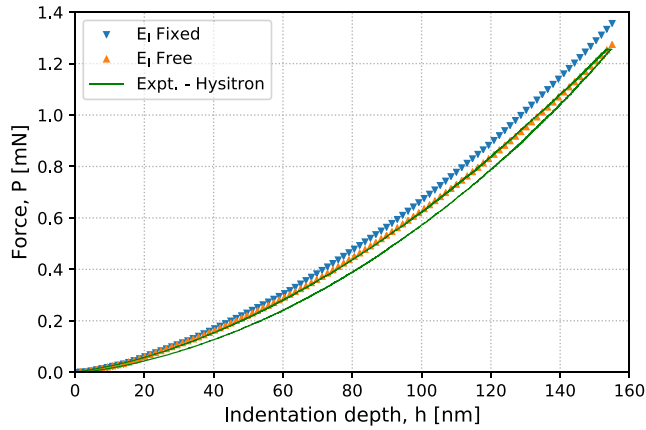


**Fig. 9.** Indentation test at 90° on IM2C carbon fibre. Comparison between experiment and FE modelling when  $E_i$  is fixed or free. (A colour version of this figure can be viewed online.)

**Table 2**

Comparison of indentation moduli in longitudinal ( $M_0$ ) and transverse directions ( $M_{90}$ ) with literature. Axial modulus values ( $E_i$ ) are also added. All values are in GPa. Values with (\*) are corrected from the original reference.

Fibre name	$M_0$	$M_{90}$	$E_i$	Technique
UTS50	81.6 ± 4.0	30.9 ± 1.5	240	
IM2C	82.1 ± 3.3	26.6 ± 1.1	296	This work
HR40	67.8 ± 2.4	21.2 ± 1.2	375	"0°" is around 14°
K637	42.1 ± 1.2	12.1 ± 1.2	640	
T300	75.9 ± 4.3	30.2 ± 1.8	237	Nanoindentation [10] "0°" is around 15°
IMS65	54.3 ± 1.3	24.6 ± 0.7	290	
T800	31.1 ± 0.9	13.7 ± 0.1	294	Nanoindentation [11]
M60J	37.5 ± 0.8	17.4 ± 0.3	588	
IMS65	106 ± 8.0	25.2 ± 1.2	290	AFM [11]
T800	90.5 ± 7.6	13.8 ± 0.6	294	
M60J	111 ± 15	17.8 ± 0.7	588	
M40J	–	15.0 ± 4.9	377 (*)	Nanoindentation [7]
M46J	–	14.0 ± 5.7	436 (*)	
K637	–	10.7 ± 3.1	640	

**Table 3**

Comparison of transverse ( $E_T$ ) and shear moduli ( $G_{lt}$ ) with literature. Axial modulus values ( $E_i$ ) are also added. All values are in GPa. SM, IM, HM and UHM stand, respectively, for Standard modulus, Intermediate Modulus, High Modulus, Ultra High Modulus carbon fibres.

Fibre name	Fibre type	$E_i$	$E_T$	$G_{lt}$	Techniques
$E_i$ fixed					
UTS50	SM	240	32.1	9.8	Nanoindentation (This work)
IM2C	IM	296	26.3	8.1	
HR40	HM	375	26.8	4.6	
K637	UHM (MPP)	640	21.2	1.2	
$E_i$ free					
UTS50	SM	130	24.3	23.4	Nanoindentation (This work)
IM2C	IM	133	17.7	25.9	
HR40	HM	116	14.5	22.9	
K637	UHM (MPP)	73.5	9.6	13.2	
T300	SM	237	27.6	10.9	Nanoindentation Csanádi et al [10].
IMS65	IM	290	21.8	12.5	AFM
T800	IM	294	14	8.7	Duan et al [11].
M60J	UHM	588	17	5.8	
IM7	IM	276	26	20.7	Composite properties
AS4	SM	231	29.9	32.2	[35]

#### 4.2. Using the extracted elastic parameters to estimate the elastic constants of continuous fibres composites

The discrepancy between the reported values for  $G_{lt}$  from Refs [10,11,35] made us question their relevance. To address this issue, we will estimate the elastic constants of a unidirectional ply of a continuous carbon fibre reinforced polymer with these carbon fibres elastic properties. The polymer matrix chosen is the epoxy resin Gurit Se84LV whose elastic constants have been determined experimentally in previous works [34,36] and reported in the supplier's datasheet [37]: Young's modulus of 3.9 GPa and Poisson's ratio of 0.4. The elastic behaviour of carbon fibres is again assumed transversely isotropic with five elastic constants  $E_l$ ,  $E_t$ ,  $G_{lt}$ ,  $\nu_{lt}$ , and  $\nu_t$ . The first value will come from the supplier's datasheet, the two following ones are the values extracted by nanoindentation. The Poisson's ratios are chosen in line with Ref. [35] ( $\nu_{lt} = 0.25$  and  $\nu_t = 0.35$ ) but they are known to be of little influence on the ply properties [10,26]. The Gurit datasheet of Se84LV resin gives also the experimentally measured elastic properties of unidirectional plies with different carbon fibres. We will use the data for SM, IM and HM PAN-based carbon fibres [19–21]. While these fibres may be strictly speaking different from the fibres we have used, they are nevertheless very similar in terms of elastic properties. We also use the fibre volume fraction of Gurit's datasheet which gives an elastic constant of interest for the ply: the transverse elastic modulus  $E_T$ . The other one, the in-plane shear modulus  $G_{LT}$ , is taken from our own experiments [36] from tensile tests on bias coupons [24] with a fibre volume fraction close to the Gurit's datasheet (at ± 3%). Meanwhile, what we are interested in are tendencies and not precise values. To compute the elastic constants, the Mori-Tanaka homogenisation scheme is used as in Ballard et al [35], with the closed-form expressions given by Abaimov et al [38].

The resulting estimated values for the three PAN-based fibres are compared with experimental ply properties ( $E_T$  and  $G_{LT}$ ). All values are reported in Table 4 (' $E_i$  fixed'). There is 18–40% in relative difference: ~ 20% for  $E_T$  and ~ 30% for  $G_{LT}$ . These large discrepancies make us assume that the extracted parameters by nanoindentation are not correct.

#### 4.3. Nano-buckling of graphene sheets during indentation and its consequences on extracting elastic parameters by indentation

The basic structural unit of carbon fibres is the graphene sheet. These sheets are preferentially arranged parallel to the carbon fibre axis. Stacks of graphene sheets form crystallites, which are arranged either randomly or rotationally symmetric with respect to the fibre axis. The most important difference between crystallites and graphite is that two adjacent sheets have neither orientational nor positional correlations. This is called the turbostratic structure [39]. The average mis-orientation of the crystallites vis-a-vis the fibre axis can be obtained by X-ray diffraction experiments (XRD, azimuthal width).

Sugimoto et al. [40] performed in situ compression of single fibres as well as XRD. They observed the occurrence of the buckling of carbon layer stacks leading to the axial compression fracture of the fibre. Cyclic compression tests indicated that the structure changes during axial compression were reversible up to 90% of the compression strength. Loidl et al. [13] bent carbon fibres under a synchrotron beam. They highlighted the existence of extensive buckling of nanocrystallites in the compression region of some MPP-based fibres. They also showed an increase of the fibre orientation (azimuthal width) upon tension and a decrease upon compression indicating bending/buckling in some PAN-based fibres.

As for indentation, Wang et al. [41] showed that the mis-

**Table 4**

Estimation of ply elastic properties using Mori-Tanaka homogenisation scheme from carbon fibre and resin matrix elastic constants. Comparison with experiments. SM, IM, and HM stand, respectively, for Standard modulus, Intermediate Modulus, High Modulus carbon fibres.

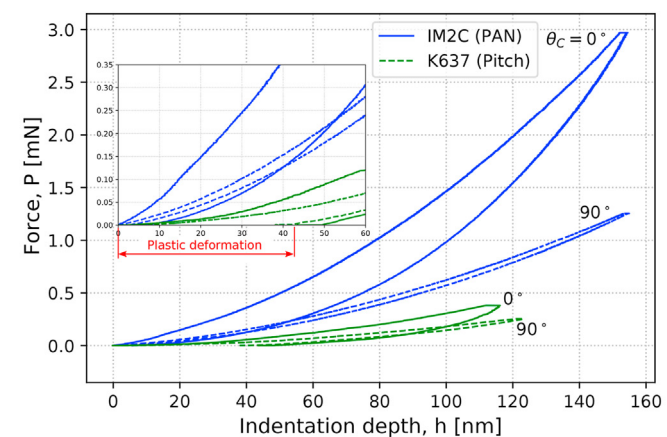
Fibre name	Fibre type	Carbon fibre properties			Ply properties (experiment)			Ply properties (Mori-Tanaka)	
		$E_l$ [GPa] $E_l$ fixed	$E_t$ [GPa]	$G_{lt}$ [GPa]	$V_f$ [%]	$E_T$ [GPa]	$G_{LT}$ [GPa]	$E_T$ [GPa]	$G_{LT}$ [GPa]
UTS50	SM	240	32.1	9.83	55.0	8.3	4.18	10.4	3.36
IM2C	IM	296	26.3	8.10	55.5	8.4	4.51	9.94	3.19
HR40	HM	375	26.8	4.63	54.4	7.1	4.22	9.82	2.54
		$E_l$ free							
UTS50	SM	130	24.3	23.4	55	8.3	4.18	9.63	4.05
IM2C	IM	133	17.7	25.9	55.5	8.4	4.51	8.78	4.16
HR40	HM	116	14.5	22.9	54.4	7.1	4.22	8.06	3.98

orientation of graphene basal planes causes continuous decrease in the indentation modulus. The difference in the mechanisms of reversible/irreversible buckling of crystallites between PAN and MPP-based fibres can also be analysed from their relevant  $P-h$  curves. Fig. 10(a) shows  $P-h$  curves for PAN (IM2C) and MPP-based fibres at orientation angles  $\theta_C$ ,  $0^\circ$  and  $90^\circ$ . For PAN-based fibres we

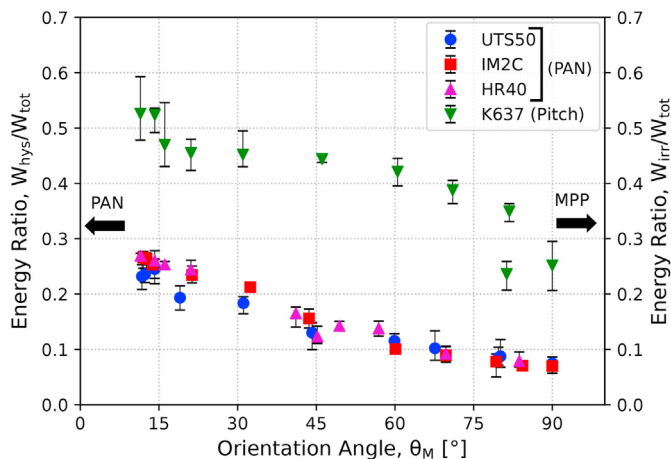
can exclude a major contribution of irreversible mechanisms. Indeed, the force-displacement curves are quasi reversible, exhibiting an hysteretic behaviour (loop). Moreover, in Fig. 5, a very shallow imprint is seen around  $\sim 5$  nm deep for  $0^\circ$  while none is observed for  $90^\circ$ . On the contrary, for MPP-based fibres, it is clear that plastic deformation occurs since irreversible depths around one third of the penetration depths are visible. We can nevertheless not exclude a possible contribution of hysteresis.

Fig. 10(b) shows the ratio of hysteresis energy to total energy with respect to the orientation angle for PAN-based fibres (UTS50, IM2C, and HR40) and the ratio of irreversible energy to total work for MPP-based fibres (K637). The hysteresis energy for PAN-based fibres and the irreversible energy for MPP-based fibres is the difference between the area under the loading curve and that under the unloading curve. The total energy is given by the area under the loading part of the curve. This energy ratio is independent of the PAN-based fibres and decreases with orientation angle, being  $\sim 25\%$  for the lowest angle and  $\sim 7\%$  for the highest. This is in line with the work of Gross et al. [42,43] who performed nano-indentation tests with different tips on pyrolytic carbon, or the earlier work of Diss et al. [44]. The same behaviour for the MPP-based fibre is observed with a ratio of  $\sim 53\%$  for the lowest orientation angle and  $\sim 25\%$  for the highest. The energy ratio is much higher for the MPP-based fibres than for the three PAN-based fibres, nearly twice as compared to the PAN-based fibres.

The procedure (see § 2.3.2) we used to extract  $E_t$  and  $G_{lt}$  and which was used in previous works by other authors [10,11] employs the axial modulus  $E_l$  taken from suppliers datasheets. These values come from tensile tests on single fibres or more commonly on bundles of fibres. The indentation modulus is sensitive to these three moduli. Yet, it was shown that buckling occurs during indentation. Therefore the axial stiffness of carbon fibres during indentation cannot be that measured during tension of single fibres and should very much be reduced due to buckling. We have consequently led the same minimisation of the cost function  $R$  (see Eq. (8)) by leaving  $E_l$  as a free parameter. In this case  $E_l$  must be seen more as a fitting parameter than as a material property. Nevertheless, we shall refer to it as a compression-like modulus of the fibre resulting from the compression mechanisms (buckling) taking place beneath the indenter tip. The new results have been added in column three to Table 1 ( $E_l$  free) and fitting curves superimposed to Fig. 8. The new fitting curves are clearly closer to experimental data points as compared to those with the minimisations made with  $E_l$  fixed. It is highly visible for IM2C (Fig. 8(a)) and K637 (Fig. 8 (d)). Table 1 shows that the error vis-a-vis the experiments (cost function  $R$ ) is indeed reduced: a little for PAN-based fibres and by almost two for the MPP fibre. The influence of the cutting angle versus the measured orientation angle on the results is also studied and results are added to Table B1 and Fig. B1.



(a)



(b)

**Fig. 10.** (a) Load versus indentation depth curves from nano-indentation tests of PAN and MPP-based fibres at  $\theta_C = 0^\circ$  and  $90^\circ$ . (b) The energy ratio (hysteresis energy/total energy for PAN and irreversible energy/total energy for MPP-based fibres) versus the orientation angle ( $\theta_M$ ) from nanoindentation experiments for four different carbon fibres. (A colour version of this figure can be viewed online.)



**Table 5**

Comparison of tensile modulus (from suppliers datasheets), compressive modulus (from this work) and mis-orientation angle ( $\varphi$ ) of both PAN and MPP-based fibres (from literature).

Fibre name	Fibre	Tens. mod.	Comp. mod.	Ratio	Fibre name	Mis-orientation
(This work)	type	$E_t^f$ [GPa]	$E_c^f$ [GPa]	$E_c^f/E_t^f$ [-]	(Ref. [46])	angle $\varphi$ [°] [46]
UTS50	PAN	240	130	0.54	T700	16.8
IM2C	PAN	296	133	0.45	IM10	15.3
HR40	PAN	375	116	0.31	UHMS	9.9
K637	MPP	640	73.5	0.11	P120	6.6

In terms of  $E_t$  and  $G_{lt}$  values, as shown in Table 3, they changed dramatically.  $E_t$  values range from 10 to 24 GPa. The higher the axial tensile modulus of the fibre, the lower  $E_t$ .  $G_{lt}$  values range from 23 to 26 GPa for PAN-based fibres, much more in line with the experimental direct results of Ishikawa et al. [5] and Kumar et al. [4]. The values are much lower for MPP-based fibre. Paris and Peterlik [39] indicate that the effective shear modulus of the crystallites is  $\sim 12$  GPa for MPP-based fibres, and is roughly twice as large for PAN-based fibres. This is in complete agreement with our values. The estimation of ply properties for these new values of  $E_t$  and  $G_{lt}$  is made (as in § 4.2) and results are added to Table 4. (Of course,  $E_l$  is taken as the tensile modulus for these estimations.) These new estimations are much closer to the experimental values than those considering  $E_l$  as the tensile modulus value. There is 3–15% in relative difference:  $\sim 10\%$  for  $E_T$  and  $\sim 5\%$  for  $G_{LT}$ .

The  $E_t$  values, resulting from this new optimisation, are shown in Table 1. They are strikingly very low:  $\sim 125$  GPa for the three PAN-based fibres and  $\sim 70$  GPa for the MPP fibre. For HR40 it is one third of the tensile modulus and for K637 it is one tenth. It is known that the compression modulus of carbon fibres decreases with compressive strain [34,45]. Ueda and Akiyama [45] showed on SM and IM PAN-based fibres that the compression behaviour is non linear elastic up to 90% of the compressive strength and that the tangent modulus decreases down to 0 at strains  $\sim 10\%$ . Due to the sharpness of the indenter tip, very high local values of compressive strains may be reached beneath the indenter in the carbon fibre during the indentation test. Oya and Johnson [3] studied the compressive behaviour of both SM and HM PAN carbon fibre using an inbuilt compression device combined with in-situ SEM. They found that the compressive modulus is nearly 50% of tensile modulus and they related the deformation mechanisms to the local crystallites buckling and kink band formation, depending on the type of fibre. Loidl et al. [13] performed micro-bending experiments using synchrotron radiation (X-Rays) to determine both tensile and compressive behaviour of PAN and MPP type fibres. They observed a shift of the neutral axis towards the tension side of the fibre. They attributed it to a progressive bending of graphene planes with applied loading for PAN-based fibres and suggested that covalent cross-links exist between the crystallites and their graphene sheets. This results in relatively high values of shear moduli. PAN-based fibres exhibit a stiffening in tension (decrease of the azimuthal angle between the fibre axis and the graphene sheets orientation) and a high softening in compression (high decrease of the azimuthal angle). For MPP-based fibres this bending degenerates into nano-buckling given the absence of covalent cross-links between the planes. This results in low shear moduli. By using a crude assumption of constant moduli in the tension and compression sides of the bent fibre, they found that the compressive modulus was less than or nearly equal to 50% of the tensile modulus for PAN

with values around 125 GPa for PAN-based fibres and  $\sim 25$  GPa for MPP-based fibres. These values are very much in line with our results. Finally, Wang et al. [47] performed uniaxial compression tests on FIB machined micropillars of three different carbon fibres (PAN type). Their results indicate that the longitudinal compression modulus is much lower than the tensile one. They also mention that elastic modulus in compression is inversely proportional to the elastic modulus in tension.

Table 5 shows the comparison of tensile modulus (from supplier datasheets) and compressive modulus (determined by indentation) of our fibres along with the mis-orientation (azimuthal width) angle of fibres with respect to their axis, having similar longitudinal tensile modulus than ours. The comparison is made with Ozcan et al. [46] data, where authors determined the mis-orientation angle ( $\varphi$ ) from X-ray diffraction measurement of both PAN and MPP type fibres. We observe that the lower the  $\varphi$  values, the lower the ratio compression modulus to tensile modulus. This ratio is in complete accordance with those reported by Loidl et al. [13].

Comparing those results of compressive modulus to the values obtained when  $E_l$  is free, we found that our values are very consistent. We consider that all our obtained values ( $E_l$ ,  $E_t$  and  $G_{lt}$ ) are thus convincing.

#### 4.4. Confrontation of the proposed approach to finite element modelling

The new sets of elastic parameters of Table 1 (' $E_l$  free') have been eventually used as input parameters for the carbon fibre in the FE modelling. Fig. 9 shows the simulation results for the transverse response of IM2C carbon fibre. The correspondance with the experiments is even better than that with the ' $E_l$  fixed' parameters. Therefore, it does strengthen our assumption of a compression-like longitudinal modulus coming into play during the indentation process linked to nano-buckling mechanisms rather than a standard tensile longitudinal modulus. It shall not be compared strictly to an axial compressive modulus measured by compression tests, but rather to an axial modulus for a given representative compressive strain, indicative of the buckling mechanisms occurring beneath the indenter tip.

## 5. Concluding remarks

Instrumented indentation testing has been used at shallow depths to characterise the mechanical behaviour of four different carbon fibres: three PAN-based fibres, with standard, intermediate and high moduli respectively, and one MPP-based fibre of ultrahigh modulus. For each type of fibre, samples were tested with 10 orientation angles between  $0^\circ$  and  $90^\circ$  with respect to the fibre axis. The actual angle of orientation was determined by measuring

the cross sections of fibres. The indentation results show a strong anisotropic behaviour in terms of indentation modulus, indentation hardness and loading pre-factor, with higher values in the axial direction and monotonously decreasing values when increasing the orientation angle. The set of indentation moduli versus actual orientation angles has then be used by a minimisation procedure to identify some elastic constants of fibres using the solutions of the anisotropic indentation boundary-value problem of Vlassak et al. [16]. Assuming their elastic behaviour to be transversely isotropic, noting that the two Poisson's ratios have little influence on the indentation response, and using the longitudinal modulus from suppliers data sheets, the two remaining other elastic constants were determined. The use of different measured orientation angles rather than one or two assumed values for sample preparation was found to be decisive.

The determined values of the transverse modulus and of the in-plane shear modulus have been found to be in line with those available in the literature using more or less the same methodology. However, especially for the shear modulus, these values are not in agreement with other reported values using different experimental techniques. Moreover, we showed that using these values and a micro-mechanical model, the estimated elastic ply properties of an epoxy matrix reinforced with these fibres are very different from experimentally reported values, particularly the in-plane shear modulus and the transverse modulus of the ply.

Based on the reported buckling of crystallites during compression in the literature, it was assumed that the longitudinal axial modulus at stake during nano-indentation was not the one measured during tensile testing on single fibres or bundles or fibres. The presence of hysteretic behaviour in our experiments for PAN-based fibres and residual impressions for the MPP-based fibre supports the assumption that buckling with moderate damage occurs for the former and severe buckling with much more damage takes place for the latter. Therefore a second minimisation was led with this time three elastic moduli of carbon fibres instead of two. The new results were very much in accordance with literature values for the transverse modulus and the in-plane shear modulus. The estimated ply properties of epoxy matrix composites were also in much better agreement with reported experiments. The identified longitudinal elastic modulus was found to be very low compared to the tensile one but in excellent agreement with reported values of compressive moduli during bending of carbon fibres. Additional comparison between the experimental transverse indentation response and Finite Element Analyses of this test using the identified elastic parameters resulted in a perfect correspondance.

This study has therefore presented the limits of using nano-indentation to identify the elastic properties of carbon fibres, when considering the longitudinal modulus as the tensile one. Nevertheless, we have proposed an improved method to remove these difficulties by considering this longitudinal modulus as a free parameter during the identification, acting more like a compression modulus mimicking the buckling of crystallites inside the carbon fibre ultrastructure beneath the indenter tip. The two other identified elastic constants, the transverse modulus and the in-plane

shear modulus, which are very difficult to measure experimentally otherwise, can therefore be extracted with our improved method.

### CRediT authorship contribution statement

**T.S. Guruprasad:** Methodology, Data curation, Investigation, Formal analysis, Writing - original draft. **V. Keryvin:** Conceptualization, Methodology, Data curation, Software, Validation, Formal analysis, Writing - original draft, Supervision, Investigation. **L. Charleux:** Software, Writing - review & editing. **J.-P. Guin:** Resources, Writing - review & editing. **O. Arnould:** Software, Writing - review & editing.

### Declaration of competing interest

The authors declare that they have no known competing interests or personal relationships that could have appeared to influence the work reported in this paper.

### Acknowledgements

We will would like to thank K. Daniel, A. Picaud, M. Grabow, A. Bourmaud, A. Magueresse (Univ. Bretagne Sud) and M. Nivard, G. Trenvoux (Univ. Rennes 1) for experimental assistance. P. Davies (IFREMER, France), P. Casari (Univ. Nantes, France) and Avel Robotics (Lorient, France) are acknowledged for providing us with some specimens. Région Bretagne and Univ. Bretagne Loire are acknowledged (INDIFIBRE project). The European Union, the French Ministry for Higher education, the Brittany region and Rennes Métropole through the CPER Projects PRIN2TAN and GLASS are finally acknowledged.

### Appendix C. Supplementary data

Supplementary data to this article can be found online at <https://doi.org/10.1016/j.carbon.2020.09.052>.

### Appendix A

In this appendix we compare the estimations of the indentation modulus ( $M$ ) given by Vlassak et al. [16] and Delafargue and Ulm [15]. This is made by choosing a test material which elastic constants (longitudinal modulus  $E_l$ , transverse modulus  $E_t$ , in-plane shear modulus  $G_{lt}$  and Poisson's ratios  $\nu_{ll}$  and  $\nu_{tt}$ ) are given in Table A1. This material has a transversely isotropic elastic behaviour.

**Table A1**  
Elastic parameters of a transversely isotropic material (high modulus carbon fibre).

$E_l$ [GPa]	$E_t$ [GPa]	$G_{lt}$ [GPa]	$\nu_{ll}$ [-]	$\nu_{tt}$ [-]
367	14.8	24	0.226	0.201

**Table A2**

Comparison between indentation modulus ( $M$ , in GPa) estimations following Vlassak et al. complete solution and circular contact approximation [16] as well as Delafargue and Ulm approximate solution [15] for the transversely isotropic material from Table A1. Orientation angles  $\theta$  of 0 and 90° are considered.

$\theta$ [°]	Vlassak et al. solution [16]		Delafargue and Ulm solution [15]	
	Complete	Circular contact approximation	Approximation	
0	146.91	146.72	146.99	
90	21.19	21.19	20.96	

We have implemented the complete solution of Vlassak et al [16], as well as two approximate estimations, the complete solution assuming a circular contact and the equivalent isotropic indenter. We have also implemented the approximate solutions of Delafargue and Ulm [15] for an orthotropic elastic behaviour and for a transversely isotropic material. The complete solution assuming either an elliptical or a circular contact from Vlassak et al [16], and the transversely isotropic approximation from Delafargue and Ulm [15] can be found as a supplementary data.

The comparison between these three estimations is shown in Table A2 for two normal indentations: at 0 and 90° with respect to the fibre axis.

The comparison between the complete solution (where an elliptical contact is assumed) and its approximation (circular contact) of Vlassak et al. [16] shows that there are no differences up to the fourth digit. As for the Delafargue and Ulm [15] approximate solution [15], it is close to these former values and identical at the second digit.

This comparison shows that using the approximate complete solution of Vlassak et al. [16] assuming a circular contact is accurate enough. Besides the computation is much faster (11.6 s versus 6 min 17 s for both angles, see supplementary material) which is necessary when reverse analyses for identifying elastic parameters are conducted.

## Appendix B

Here, we present a comparative study on the influence of the cutting angle versus the measured orientation angle of the fibres on the elastic constants. The orientation of the actual angle of the fibre ( $\theta_M$ ) is necessary, as the error in the orientation angle leads to an error in the values of the elastic constants. A comparative study of cutting ( $\theta_C$ ) versus measured ( $\theta_M$ ) orientation angles on the indentation modulus is shown in Fig. B1 for IM2C fibre. There exists a difference between the two such that it cannot be neglected. The better fits are obtained when the considered orientation angle is the measured angle. The corresponding values of the elastic constants and the error are shown in Table B1. The determined values of  $E_t$  and  $G_{lt}$  are slightly different between the two types of angles. Also, errors obtained from minimisation are more than two times higher for the cutting angle compared to the measured angle. Thus, to obtain the correct values of the elastic constants, it is very important to measure the real angle, otherwise large errors could affect the results.

**Table B1**

Elastic constants determined from minimisation of a cost function R, see Eq. (8), for IM2C fibre, and its error R with respect to the experimental values, when  $E_l$  is fixed (left side) or free (right side). Comparison between the use of the orientation angle when it is the cutting one ( $\theta_C$ ) and when it is measured from SEM images ( $\theta_M$ ). All the elastic constant values are in GPa.

Angle	$E_l$ is fixed, $E_t$ and $G_{lt}$ are free				$E_l, E_t$ and $G_{lt}$ are free			
	$E_l$	$E_t$	$G_{lt}$	Error, R (%)	$E_l$	$E_t$	$G_{lt}$	Error, R (%)
Measured ( $\theta_M$ )	296	26.3	8.1	6.0	133	17.7	25.9	4.0
Cut ( $\theta_C$ )	296	30.2	7.5	14.3	108	12.1	71.8	8.7

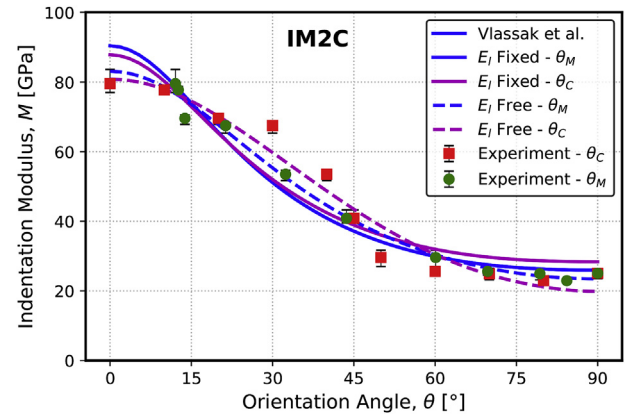


**Figure B.1.** Indentation modulus versus the orientation angle of IM2C carbon fibres when the orientation is either taken as the cutting angle ( $\theta_C$ , dashed lines) or as a measured one from SEM pictures ( $\theta_M$ , solid lines) and the respective numerical fits using Vlassak et al [16]. solutions. The dark blue lines are for the minimisation with two parameters ( $E_l$  fixed) while the purple lines are for three ( $E_l$  free).

## References

- [1] D.J. Johnson, Structure-property relationships in carbon fibres, *J. Phys. Appl. Phys.* 20 (1987) 286–291, <https://doi.org/10.1088/0022-3727/20/3/007>.
- [2] M. Northolt, L. Veldhuizen, H. Jansen, Tensile deformation of carbon fibers and the relationship with the modulus for shear between the basal planes, *Carbon* 29 (1991) 1267–1279, [https://doi.org/10.1016/0008-6223\(91\)90046-L](https://doi.org/10.1016/0008-6223(91)90046-L).
- [3] N. Oya, D.J. Johnson, Longitudinal compressive behaviour and microstructure of pan-based carbon fibres, *Carbon* 39 (2001) 635–645, [https://doi.org/10.1016/S0008-6223\(00\)00147-0](https://doi.org/10.1016/S0008-6223(00)00147-0).
- [4] I.P. Kumar, S.P. Kushwaha, P. Mohite, S. Kamle, Longitudinal shear modulus of single aramid, carbon and glass fibres by torsion pendulum tests, *Int. J. Mech. Mechatron. Eng.* 8 (2014) 423–428.
- [5] M. Ishikawa, Y. Kogo, J. Koyanagi, F. Tanaka, T. Okabe, Torsional modulus and internal friction of polyacrylonitrile- and pitch-based carbon fibers, *J. Mater. Sci.* 50 (2015).
- [6] S. Datta, H. Ledbetter, T. Kyono, Graphite-Fiber Elastic Constants: Determination from Ultrasonic Measurements on Composite Materials, Springer US, Boston, MA, 1989, pp. 1481–1488, [https://doi.org/10.1007/978-1-4613-0817-1\\_186](https://doi.org/10.1007/978-1-4613-0817-1_186).
- [7] R. Maurin, P. Davies, N. Baral, C. Baley, Transverse properties of carbon fibres by nano-indentation and micro-mechanics, *Appl. Compos. Mater.* 15 (2008) 61–73, <https://doi.org/10.1007/s10443-008-9057-3>.
- [8] H. Miyagawa, T. Mase, C. Sato, E. Drown, L.T. Drzal, K. Ikegami, Comparison of experimental and theoretical transverse elastic modulus of carbon fibers, *Carbon* 44 (2006) 2002–2008, <https://doi.org/10.1016/j.carbon.2006.01.026>.
- [9] A. Leatherbarrow, H. Wu, Mechanical behaviour of the constituents inside carbon-fibre/carbon-silicon carbide composites characterised by nano-indentation, *J. Eur. Ceram. Soc.* 32 (2012) 579–588, <https://doi.org/10.1016/j.jeurceramsoc.2011.09.026>.
- [10] T. Csanádi, D. Németh, C. Zhang, J. Duszka, Nanoindentation derived elastic constants of carbon fibres and their nanostructural based predictions, *Carbon* 119 (2017) 314–325, <https://doi.org/10.1016/j.carbon.2017.04.048>.
- [11] S. Duan, F. Liu, T. Pettersson, C. Creighton, L.E. Asp, Determination of transverse and shear moduli of single carbon fibres, *Carbon* 158 (2020) 772–782, <https://doi.org/10.1016/j.carbon.2019.11.054>.
- [12] I. Krucinska, T. Stypka, Direct measurement of the axial Poisson's ratio of single carbon fibres, *Compos. Sci. Technol.* 41 (1991) 1–12, [https://doi.org/10.1016/0266-3538\(91\)90049-U](https://doi.org/10.1016/0266-3538(91)90049-U).
- [13] D. Loidl, O. Paris, M. Burghammer, C. Riekel, H. Peterlik, Direct observation of nanocrystallite buckling in carbon fibers under bending load, *Phys. Rev. Lett.* 95 (2005) 225501, <https://doi.org/10.1103/PhysRevLett.95.225501>.
- [14] W. Oliver, G. Pharr, An improved technique for determining hardness and elastic modulus using load and displacement sensing indentation experiments, *J. Mater. Res.* 7 (1992) 1564–1583, <https://doi.org/10.1557/JMR.1992.1564>.
- [15] A. Delafargue, F.-J. Ulm, Explicit approximations of the indentation modulus of elastically orthotropic solids for conical indenters, *Int. J. Solid Struct.* 41 (2004) 7351–7360, <https://doi.org/10.1016/j.ijsolstr.2004.06.019>.
- [16] J. Vlassak, M. Ciavarella, J. Barber, X. Wang, The indentation modulus of elastically anisotropic materials for indenters of arbitrary shape, *J. Mech. Phys.*

- Solid. 51 (2003) 1701–1721, [https://doi.org/10.1016/S0022-5096\(03\)00066-8](https://doi.org/10.1016/S0022-5096(03)00066-8).
- [17] S.R. Swanson, Hertzian contact of orthotropic materials, *Int. J. Solid Struct.* 41 (2004) 1945–1959, <https://doi.org/10.1016/j.ijsolstr.2003.11.003>.
- [18] A. Jäger, K. Hofstetter, C. Buksnowitz, W. Gindl-Altmutter, J. Konnerth, Identification of stiffness tensor components of wood cell walls by means of nanoindentation, *Compos. Appl. Sci. Manuf.* 42 (2011) 2101–2109, <https://doi.org/10.1016/j.compositesa.2011.09.020>.
- [19] [www.tohotenax-eu.com](http://www.tohotenax-eu.com), 2012. <http://www.asprotec.ru/pub/UTS50.pdf>. Original document from Toho Tenax Europe GmbH.
- [20] [www.hexcel.com](http://www.hexcel.com), 2018. [https://www.hexcel.com/user\\_area/content\\_media/raw/IM2C\\_HexTow\\_DataSheet.pdf](https://www.hexcel.com/user_area/content_media/raw/IM2C_HexTow_DataSheet.pdf). Original document from Hexcel Corporation.
- [21] [www.m-chemical.co.jp](http://www.m-chemical.co.jp), 2020. [https://www.m-chemical.co.jp/en/products/departments/mcc/cfcm/product/CFtow\\_Jan2020en.pdf](https://www.m-chemical.co.jp/en/products/departments/mcc/cfcm/product/CFtow_Jan2020en.pdf). Original document from Mitsubishi chemical carbon fiber and composites.
- [22] [www.m-chemical.co.jp](http://www.m-chemical.co.jp), 2019. [https://www.900gpa.com/en/product/fiber/CF\\_00DE80C9A67u=us](https://www.900gpa.com/en/product/fiber/CF_00DE80C9A67u=us). Original document from Mitsubishi chemical carbon fiber and composites.
- [23] C. Schneider, W. Rasband, K. Eliceiri, NIH Image to ImageJ: 25 years of image analysis, *Nat. Methods* 9 (2012), <https://doi.org/10.1038/nmeth.2089>.
- [24] P.-Y. Mechin, V. Keryvin, J.-C. Grandidier, D. Glehen, An experimental protocol to measure the parameters affecting the compressive strength of CFRP with a fibre micro-buckling failure criterion, *Compos. Struct.* 211 (2019) 154–162, <https://doi.org/10.1016/j.compstruct.2018.12.026>.
- [25] L. Charleux, V. Keryvin, M. Nivard, J.P. Guin, J.C. Sangleboeuf, Y. Yokoyama, A method for measuring the contact area in instrumented indentation testing by tip scanning probe microscopy imaging, *Acta Mater.* 70 (2014) 249–258, <https://doi.org/10.1016/j.actamat.2014.02.036>.
- [26] A. Jäger, T. Bader, K. Hofstetter, J. Eberhardsteiner, The relation between indentation modulus, microfibril angle, and elastic properties of wood cell walls, *Compos. Appl. Sci. Manuf.* 42 (2011) 677–685, <https://doi.org/10.1016/j.compositesa.2011.02.007>.
- [27] M. Smith, *ABAQUS/Standard User's Manual, Version 2018*, Dassault Systèmes Simulia Corp, United States, 2018.
- [28] C. Geuzaine, J.-F. Remacle, Gmsh, A 3-D finite element mesh generator with built-in pre-and post-processing facilities, *Int. J. Numer. Methods Eng.* 79 (2009) 1309–1331, <https://doi.org/10.1002/nme.2579>.
- [29] L. Charleux, Lcharleux/Hardness: Hardness 0.4.1, 2020, <https://doi.org/10.5281/zenodo.3900104>, [10.5281/zenodo.3900104](https://doi.org/10.5281/zenodo.3900104).
- [30] L. Charleux, E. Roux, C. Bernard, lcharleux/argiope: Argiope v0.4.1. <https://doi.org/10.5281/zenodo.2932536>, 2019. [10.5281/zenodo.2932536](https://doi.org/10.5281/zenodo.2932536).
- [31] Y. Sun, G. Zhao, F. Yang, Anisotropic behavior of the nanoindentation of single carbon fibers, *Nanosci. Nanotechnol. Lett.* 6 (2014) 596–600, <https://doi.org/10.1166/nnl.2014.1809>.
- [32] Y.-T. Cheng, C.-M. Cheng, Scaling, dimensional analysis, and indentation measurements, *Mater. Sci. Eng. R Rep.* 44 (2004) 91–149, <https://doi.org/10.1016/j.mser.2004.05.001>.
- [33] V. Keryvin, L. Charleux, C. Bernard, M. Nivard, The influence of indenter tip imperfection and deformability on analysing instrumented indentation tests at shallow depths of penetration on stiff and hard materials, *Exp. Mech.* 57 (2017) 1–7, <https://doi.org/10.1007/s11340-017-0267-1>.
- [34] V. Keryvin, A. Marchandise, P.-Y. Mechin, J.-C. Grandidier, Determination of the longitudinal non linear elastic behaviour and compressive strength of a CFRP ply by bending tests on laminates, *Compos. B Eng.* 187 (2020) 107863, <https://doi.org/10.1016/j.compositesb.2020.107863>.
- [35] M.K. Ballard, W.R. McLendon, J.D. Whitcomb, The influence of microstructure randomness on prediction of fiber properties in composites, *J. Compos. Mater.* 48 (2014) 3605–3620, <https://doi.org/10.1177/0021998313511654>.
- [36] P.-Y. Mechin, V. Keryvin, J.-C. Grandidier, Limitations on adding nano-fillers to increase the compressive strength of continuous fibre/epoxy matrix composites, *Compos. Sci. Technol.* 192 (2020) 108099, <https://doi.org/10.1016/j.compscitech.2020.108099>.
- [37] [www.gurit.com](http://www.gurit.com), 2012. <https://www.gurit.com/-/media/Gurit/Datasheets/se-84lv.PDF> (Original document from Gurit.com).
- [38] S.G. Abaimov, A.A. Khudyakova, S.V. Lomov, On the closed form expression of the mori–tanaka theory prediction for the engineering constants of a unidirectional fiber-reinforced ply, *Compos. Struct.* 142 (2016) 1–6, <https://doi.org/10.1016/j.compstruct.2016.02.001>.
- [39] O. Paris, H. Peterlik, *Single Carbon Fibres: Structure from X-Ray Diffraction and Nanomechanical Properties*, Springer Vienna, Vienna, 2016, pp. 1–28, [https://doi.org/10.1007/978-3-7091-1887-0\\_1](https://doi.org/10.1007/978-3-7091-1887-0_1).
- [40] Y. Sugimoto, T. Kato, M. Shioya, T. Kobayashi, K. Sumiya, M. Fujie, Structure change of carbon fibers during axial compression, *Carbon* 57 (2013) 416–424, <https://doi.org/10.1016/j.carbon.2013.02.014>.
- [41] H. Wang, H. Zhang, D. Tang, K. Goto, I. Watanabe, H. Kitazawa, M. Kawai, H. Mamiya, D. Fujita, Stress dependence of indentation modulus for carbon fiber in polymer composite, *Sci. Technol. Adv. Mater.* 20 (2019) 412–420, <https://doi.org/10.1080/14686996.2019.1600202>.
- [42] T. Gross, N. Timoshchuk, I. Tsukrov, R. Piat, B. Reznik, On the ability of nanoindentation to measure anisotropic elastic constants of pyrolytic carbon, *ZAMM J. Appl. Math. Mech.: Zeitschrift für angewandte Mathematik und Mechanik* 93 (2013), <https://doi.org/10.1002/zamm.201100128>.
- [43] T. Gross, N. Timoshchuk, I. Tsukrov, B. Reznik, Unique nanoindentation damage for highly textured pyrolytic carbon, *Carbon* 60 (2013) 273–279, <https://doi.org/10.1016/j.carbon.2013.04.036>.
- [44] P. Diss, J. Lamon, L. Carpentier, J. Loubet, P. Kapsa, Sharp indentation behavior of carbon/carbon composites and varieties of carbon, *Carbon* 40 (2002) 2567–2579, [https://doi.org/10.1016/S0008-6223\(02\)00169-0](https://doi.org/10.1016/S0008-6223(02)00169-0).
- [45] M. Ueda, M. Akiyama, Compression test of a single carbon fiber in a scanning electron microscope and its evaluation via finite element analysis, *Adv. Compos. Mater.* 28 (2019) 57–71, <https://doi.org/10.1080/09243046.2018.1433506>.
- [46] S. Ozcan, F. Vautard, A.K. Naskar, Designing the Structure of Carbon Fibers for Optimal Mechanical Properties, 2014, pp. 215–232, <https://doi.org/10.1021/bk-2014-1173.ch010>.
- [47] J. Wang, N. Salim, B. Fox, N. Stanford, Anisotropic compressive behaviour of turbostratic graphite in carbon fibre, *Appl. Mater. Today* 9 (2017) 196–203, <https://doi.org/10.1016/j.apmt.2017.07.010>.